XML-IS

Our reference: MS 2123 P-authorquery-vx

AUTHOR QUERY FORM

ELSEVIER	**Journal: MS** **Article Number: 2123**	**Please e-mail or fax your responses and any corrections to:** **E-mail: corrections.esch@elsevier.macipd.com** **Fax: +44 1392 285878**

Dear Author,

Please check your proof carefully and mark all corrections at the appropriate place in the proof (e.g., by using on-screen annotation in the PDF file) or compile them in a separate list.

For correction or revision of any artwork, please consult http://www.elsevier.com/artworkinstructions.

Any queries or remarks that have arisen during the processing of your manuscript are listed below and highlighted by flags in the proof. Click on the Q link to go to the location in the proof.

Location in article	**Query / Remark: click on the Q link to go** **Please insert your reply or correction at the corresponding line in the proof**
Q1	Please check the telephone/fax number of the corresponding author, and correct if necessary.
Q2	The number of keywords provided exceeds the maximum allowed by this journal. Please delete 1 keyword.

Thank you for your assistance.

Contents lists available at ScienceDirect

International Journal of Mechanical Sciences

journal homepage: www.elsevier.com/locate/ijmecsci

Highlights

International Journal of Mechanical Sciences ∎ (∎∎∎∎) ∎∎∎–∎∎∎

Scattering of flexural wave in a thin plate with multiple circular inclusions by using the multipole method

W.M. Lee [a], J.T. Chen [b]

Q1 [a] *Department of Mechanical Engineering, China University of Science and Technology, Taipei, Taiwan*
[b] *Department of Harbor and River Engineering, National Taiwan Ocean University, Keelung, Taiwan*

► Scattering of flexural wave by multiple circular inclusions was analytically solved. ► Dynamic moment concentration factor and scattering pattern were both investigated. ► Scattering pattern can be used to detect the size and severity of structural anomaly. ► The magnitude of DMCF mainly depends on the separation of damage. ► The effect of separation on the DMCF is opposite to that on the scattering pattern.

doi:10.1016/j.ijmecsci.2011.05.008

International Journal of Mechanical Sciences ∎ (∎∎∎∎) ∎∎∎–∎∎∎

Contents lists available at ScienceDirect

International Journal of Mechanical Sciences

journal homepage: www.elsevier.com/locate/ijmecsci

Scattering of flexural wave in a thin plate with multiple circular inclusions by using the multipole method

W.M. Lee [a,*], J.T. Chen [b]

Q1 [a] Department of Mechanical Engineering, China University of Science and Technology, Taipei, Taiwan
[b] Department of Harbor and River Engineering, National Taiwan Ocean University, Keelung, Taiwan

ARTICLE INFO

Article history:
Received 13 June 2010
Received in revised form
18 May 2011
Accepted 19 May 2011

Q2 *Keywords:*
Scattering
Plate
Circular inclusion
Flexural wave
Dynamic moment concentration factor
Far-field scattering pattern
Addition theorem

ABSTRACT

The multipole method is presented to analytically solve the scattering of flexural wave by multiple circular inclusions in an infinite thin plate. The near-field dynamic moment concentration factor (DMCF) and the far-field scattering pattern are both investigated in this paper. The former has a connection with the fatigue failures and the damages in plate-like structures can be detected by the latter. Owing to the addition theorem, the multipole expansion for the multiple scattering fields can be transformed into one coordinate system centered at one circle where continuity conditions are required. In this way, a coupled infinite linear algebraic system is derived as an analytical model for an infinite thin plate with multiple circular inclusions subject to an incident flexural wave. The convergence analysis is conducted to provide the guideline of usage for the proposed method. The effects of the size and thickness of the flexible inclusion, and the central distance between inclusions on the near-field DMCF and the far-field scattering pattern are investigated in the numerical experiments. It shows that the scattering pattern correlates closely with the size and thickness of damages, indicating the importance of the scattering pattern to detect the various damages. In addition, the DMCF of two corrosion damages is larger than that of one. Therefore, it is essential to evaluate structural safety when multiple circular defects are very close to each other. The effect of the space between the inclusions on the near-field DMCF is different from that on the far-field scattering pattern.

1. Introduction

Thin plates with multiple circular inclusions are commonly observed in many practical engineering structures. These inclusions, or inhomogeneities, usually take place in terms of either the thickness reduction due to corrosion in a metallic plate or the strength degradation caused by delamination in a quasi-isotropic composite plate. The other examples can be found in the plates with bolts or rivets, which are often used in the engineering structure. The deformation and corresponding stresses induced by dynamic loading are propagated throughout the structure by means of wave. At the near field of inclusion (or obstacle), flexural wave scattered in all directions recursively interacts with the incident wave. It turns out that the scattering of the stress wave induces dynamic stress concentration [1], which results in fatigue failure and reduces the loading capacity. On the other hand, the far-field scattering pattern can determine the size and severity of structural damages in plate-like structure by using a quantitative in situ structural health-monitoring system, one of the non-destructive inspections.

One of the early research studies in the analytical approach to the dynamic stress concentrations is that of Nishimura and Jimbo [2]. The stresses in the vicinity of a spherical inclusion in the elastic solid under a harmonic force were investigated. Pao [3] studied the scattering of flexural waves and dynamic stress concentrations around a circular hole, and proposed an analytical solution. Thau and Lu [4] studied the dynamic stress concentration at a cylindrical inclusion in an elastic medium. Since then, most research work has focused on the scattering of elastic wave and the resulted dynamic stress concentration, and has led to a rapid development of analytical or numerical approach such as the method of wave function expansion, the complex variable method, the boundary integral equation method and the boundary element method [1].

Norris and Vemula [5] considered the scattering of flexural waves by circular inclusions with different plate properties and obtained numerical results. Squire and Dixon [6] applied the wave function expansion method to study the scattering properties of a single coated cylindrical anomaly located in a thin plate on which flexural waves propagate. Wang and Chang [7] presented a theoretical and experimental investigation of the scattering

* Corresponding author. Tel.: +886 2 27867048; fax: +886 2 27867253
E-mail address: wmlee@cc.cust.edu.tw (W.M. Lee).

0020-7403/$ - see front matter © 2011 Elsevier Ltd. All rights reserved.
doi:10.1016/j.ijmecsci.2011.05.008

Please cite this article as: Lee WM, Chen JT. Scattering of flexural wave in a thin plate with multiple circular inclusions by using the multipole method. International Journal of Mechanical Sciences (2011), doi:10.1016/j.ijmecsci.2011.05.008

behavior of extensional and flexural plate waves by a cylindrical inhomogeneity. Peng [8] investigated flexural wave scattering and dynamic stress concentration in a heterogeneous plate with multiple cylindrical patches by using acoustical wave propagator technique. Recently Lee and Chen [9] proposed a semi-analytical approach to solve the flexural wave scattered by multiple circular inclusions in an infinite plate by using the null-field integral equation method. In addition to the need of integration, this collocation method belongs to a point-matching approach instead of an analytical one. It also increases the effort of computation since boundary nodes for collocation are required.

The concept of multipole method to solve multiply-connected domain problems was firstly devised by Zàviška [10] and used for the interaction of waves with arrays of circular cylinders by Linton and Evans [11]. In this paper, we extend it to the scattering of flexural weave in an infinite thin plate with multiple circular inclusions. By using the addition theorem and matching the continuity conditions at the interface of the inclusions, a coupled infinite system of simultaneous linear algebraic equations is derived as an analytical model for the title problem. Finally some numerical results are presented in the truncated finite system. Once the displacement fields of each inclusion and the surrounding plate are solved, the near-field DMCF and the far-field scattering pattern can be determined in a theoretical way. The effects of the size and thickness of the flexible inclusion, and the space between inclusions on the near-field DMCF and the far-field scattering pattern, respectively, are examined in this paper.

2. Problem statement and the general solution

An infinite thin plate containing H circular inclusions with different thickness from the surrounding plate, subjected to the incident flexural wave is shown in Fig. 1, where $H+1$ observer coordinate systems are used: (x_1, x_2) are the global plane Cartesian coordinates centered at O (ρ_p, ϕ_p), $p=1, \ldots, H$ are local plane polar coordinates centered at O_p, R_p denotes the radius of the pth circular inclusion, h_p and B_p are its corresponding boundary and thickness.

When considering the time-harmonic motion exclusively, the governing equation of the flexural wave for a uniform infinite thin plate with distributed circular inclusions as shown in Fig. 1 is

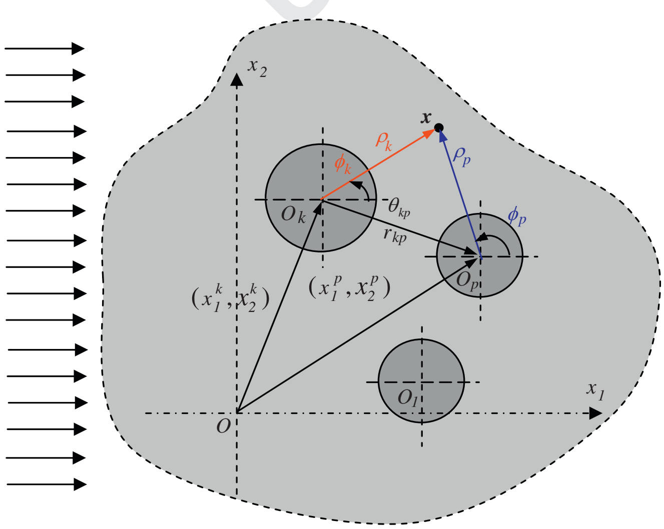

Fig. 1. Problem statement for an infinite thin plate with multiple circular inclusions subject to an incident flexural wave.

written as follows:

$$\nabla^4 w(\boldsymbol{x}) - k^4 w(\boldsymbol{x}) = 0, \quad \boldsymbol{x} \in \Omega^e, \tag{1}$$

where ∇^4 is the biharmonic operator, $w(\boldsymbol{x})$ is the out-of-plane elastic displacement and $\boldsymbol{x}$ is the field point, Ω^e is the unbounded exterior region occupied by the infinite plate, $k^4 = \omega^2 \rho_0 h/D$, $k(2\pi/$wave length) is the wave number of elastic wave, ω is the circular frequency, ρ_0 is the volume density, $D = Eh^3/12(1-\mu^2)$ is the flexural rigidity, E denotes Young's modulus, μ is Poisson's ratio and h_0 is the plate thickness.

The solution of the Bi-Helmholtz equation, Eq. (1), in the plane polar coordinates can be represented as

$$w(\rho, \phi) = \sum_{m=-\infty}^{\infty} \tilde{w}_m(\rho) e^{im\phi}, \tag{2}$$

where $\tilde{w}_m(\rho)$ is defined by

$$\tilde{w}_m(\rho) = c_m^1 J_m(k\rho) + c_m^2 Y_m(k\rho) + c_m^3 I_m(k\rho) + c_m^4 K_m(k\rho), \tag{3}$$

in which c_m^i $(i=1-4)$ are the coefficients, J_m and Y_m are the mth order Bessel functions; and I_m and K_m are the mth order modified Bessel functions. Based on the characteristics of functions at $\rho=0$ and $\rho \to \infty$, the appropriate Bessel function and the modified Bessel function are chosen to represent the transverse displacement field for the infinite plate and finite inclusion.

When harmonic forces are applied perpendicularly to a thin plate and they are far enough from the inclusions, an incident flexural wave with an incident wave number k and angle α with respect to the x_1-axis can be represented by

$$w(\boldsymbol{x}) = w_0 e^{i(x_1 \cos\alpha + x_2 \sin\alpha)k}, \tag{4}$$

where w_0 is the amplitude of the incident wave. By substituting $x_1 = x_1^p + \rho_p \cos(\phi_p)$ and $x_2 = x_2^p + \rho_p \sin(\phi_p)$ into Eq. (4), the incident flexural wave in the pth circular inclusion is given by

$$w^{(i)}(\rho_p, \phi_p) = w_0 c_p e^{ik\rho_p \cos(\phi_p - \alpha)}, \quad p = 1, \ldots, H, \tag{5}$$

where $c_p = e^{ik(x_1^p \cos\alpha + x_2^p \sin\alpha)}$ is a phase factor associated with the pth circular inclusion [11]. From Jacobi's expansion [12], $e^{ix\cos\phi} = \sum_{m=-\infty}^{\infty} i^m J_m(x) e^{im\phi}$, Eq. (5) can be expanded in a series form

$$w^{(i)}(\rho_p, \phi_p) = \sum_{m=-\infty}^{\infty} a_m^{(i)}(k\rho_p) e^{im\phi_p}, \quad p = 1, \ldots, H, \tag{6}$$

where $a_m^{(i)}(k\rho_p) = w_0 c_p i^m J_m(k\rho_p) e^{-im\alpha}$.

Based on the displacement field, the slope, the bending moment, the tangential bending moment and the effective shear force can be derived by applying the following operators with respect to the field point:

$$K_\Theta(\cdot) = \frac{\partial(\cdot)}{\partial\rho}, \tag{7}$$

$$K_{m_n}(\cdot) = -D\left[\mu\nabla^2(\cdot) + (1-\mu)\frac{\partial^2(\cdot)}{\partial\rho^2}\right], \tag{8}$$

$$K_{m_t}(\cdot) = -D\left[\nabla^2(\cdot) + (\mu-1)\frac{\partial^2(\cdot)}{\partial\rho^2}\right], \tag{9}$$

$$K_v(\cdot) = -D\left[\frac{\partial}{\partial\rho}(\nabla^2(\cdot)) + (1-\mu)\left(\frac{1}{\rho}\right)\frac{\partial}{\partial\phi}\left[\frac{\partial}{\partial\rho}\left(\frac{1}{\rho}\frac{\partial(\cdot)}{\partial\phi}\right)\right]\right]. \tag{10}$$

3. Analytical derivations for flexural wave scattered by multiple circular inclusions in a thin plate

Assume that a time-harmonic incident flexural wave impinges on an infinite thin plate containing H circular inclusions as shown in Fig. 1. The problem of flexural wave scattered by H circular inclusions is to solve Eq. (1) subject to continuity conditions along each interface between the plate and inclusions and a radiation condition at infinity, i.e. the scattered field decaying as $\rho^{-1/2}$ (or approaching to zero when $\rho \to \infty$). Based on Eq. (3), the scattered field of plate can be expressed as an infinite sum of multipoles at the center of each circular inclusion as follows:

$$w^{(sc)}(\boldsymbol{x};\rho_1,\phi_1,\ldots,\rho_H,\phi_H) = \sum_{k=1}^{H}\left[\sum_{m=-\infty}^{\infty} a_m^k H_m^{(1)}(k\rho_k)e^{im\phi_k} + b_m^k K_m(k\rho_k)e^{im\phi_k}\right], \quad (11)$$

where (ρ_1,ϕ_1), …, (ρ_H,ϕ_H) are the polar coordinates of the field point $\boldsymbol{x}$ with respect to each center of circular inclusion. The Hankel function of the first kind $(J+iY)$ and the modified Bessel function K are chosen to represent an infinite plate due to their finite values and outgoing propagation as $\rho \to \infty$. Considering the incident wave, the total displacement field of the plate is defined by

$$w(\boldsymbol{x}) = w^{(i)}(\boldsymbol{x}) + w^{(sc)}(\boldsymbol{x}). \quad (12)$$

Similarly, from Eq. (3), the displacement field of the pth inclusion can be expressed as

$$w_p^i(\boldsymbol{x};\rho_p,\phi_p) = \sum_{m=-\infty}^{\infty}\left(c_m^p J_m(k\rho_p)e^{im\phi_p} + d_m^p I_m(k\rho_p)e^{im\phi_p}\right) \quad (13)$$

for $p=1,\ldots,H$. The Bessel function J and the modified Bessel function I are chosen to represent a finite inclusion due to their finite values at $\rho=0$.

The coefficients of a_m^k, b_m^k, c_m^k and d_m^k, $k=1,\ldots,H$; $m=0,\ \pm 1,\ \pm 2,\ \ldots$ can be determined by the following continuity conditions at each interface, $0 \le \phi_p \le 2\pi$, $p=1,\ldots,H$

$$w(\rho_p,\phi_p) = w_p^i(\rho_p,\phi_p)\Big|_{\rho_p=R_p}, \quad (14)$$

$$\theta(\rho_p,\phi_p) = \theta_p^i(\rho_p,\phi_p)\Big|_{\rho_p=R_p}, \quad (15)$$

$$m(\rho_p,\phi_p) = m_p^i(\rho_p,\phi_p)\Big|_{\rho_p=R_p}, \quad (16)$$

$$v(\rho_p,\phi_p) = v_p^i(\rho_p,\phi_p)\Big|_{\rho_p=R_p}. \quad (17)$$

For the pth circular interface, substituting both Eqs. (12) and (13) into Eq. (14) yields

$$\sum_{m=-\infty}^{\infty} a_m^{(i)}(k\rho_p)e^{im\phi_p} + \sum_{k=1}^{H}\left[\sum_{m=-\infty}^{\infty} a_m^k H_m^{(1)}(k\rho_k)e^{im\phi_k} + b_m^k K_m(k\rho_k)e^{im\phi_k}\right] - \sum_{m=-\infty}^{\infty}\left(c_m^p J_m(k\rho_p)e^{im\phi_p} + d_m^p I_m(k\rho_p)e^{im\phi_p}\right)\Big|_{\rho_p=R_p} = 0. \quad (18)$$

To determine these unknown coefficients, the other three Eqs. (15)–(17) are required by applying three operators of Eqs. (7), (8) and (10) into Eq. (18). Not only does this procedure involve the higher-order derivatives, Eq. (18) also involves multi-variables. Therefore, it is difficult to determine the unknown coefficients by using the procedure mentioned above. This problem can be solved by using the addition theorem [12], which can convert multi-variables into one variable so that the higher-order derivatives can be easily determined.

Graf's addition theorem for the Bessel function can be expressed as follows:

$$J_m(k\rho_k)e^{im\phi_k} = \sum_{n=-\infty}^{\infty} J_{m-n}(kr_{kp})e^{i(m-n)\theta_{kp}}J_n(k\rho_p)e^{in\phi_p}, \quad (19)$$

$$I_m(k\rho_k)e^{im\phi_k} = \sum_{n=-\infty}^{\infty} I_{m-n}(kr_{kp})e^{i(m-n)\theta_{kp}}I_n(k\rho_p)e^{in\phi_p}, \quad (20)$$

$$H_m^{(1)}(k\rho_k)e^{im\phi_k} = \sum_{n=-\infty}^{\infty} H_{m-n}^{(1)}(kr_{kp})e^{i(m-n)\theta_{kp}}J_n(k\rho_p)e^{in\phi_p}, \quad (21)$$

$$K_m(k\rho_k)e^{im\phi_k} = \sum_{n=-\infty}^{\infty} (-1)^n K_{m-n}(kr_{kp})e^{i(m-n)\theta_{kp}}I_n(k\rho_p)e^{in\phi_p}, \quad (22)$$

for $\rho_p < r_{kp}$, where (ρ_p,ϕ_p) and (ρ_k,ϕ_k) as shown in Fig. 1 are the polar coordinates of the field point $\boldsymbol{x}$ with respect to O_p and O_k, respectively, which are the origins of two polar coordinate systems and (r_{kp},θ_{kp}) are the polar coordinates of O_p with respect to O_k.

By substituting the addition theorem for the Bessel functions $H_m^{(1)}(k\rho_k)$ and $K_m(k\rho_k)$ into Eq. (18), only the pth coordinates are involved and then the displacement continuity condition in the circular boundary B_p $(p=1,\ldots,H)$ is given by

$$\sum_{m=-\infty}^{\infty} a_m^{(i)}(k\rho_p)e^{im\phi_p} + \left[\sum_{m=-\infty}^{\infty} a_m^p H_m^{(1)}(k\rho_p) + \sum_{m=-\infty}^{\infty} b_m^p K_m(k\rho_p)\right]e^{im\phi_p} + \sum_{\substack{k=1\\k\neq p}}^{H}\left[\sum_{m=-\infty}^{\infty} a_m^k \sum_{n=-\infty}^{\infty} H_{m-n}^{(1)}(kr_{kp})e^{i(m-n)\theta_{kp}}J_n(k\rho_p) + \sum_{m=-\infty}^{\infty} b_m^k \sum_{n=-\infty}^{\infty} (-1)^n K_{m-n}(kr_{kp})e^{i(m-n)\theta_{kp}}I_n(k\rho_p)\right]e^{in\phi_p} - \sum_{m=-\infty}^{\infty}\left(c_m^p J_m(k\rho_p)e^{im\phi_p} + d_m^p I_m(k\rho_p)e^{im\phi_p}\right)\Big|_{\rho_p=R_p} = 0. \quad (23)$$

Furthermore, it can be rewritten as

$$\sum_{m=-\infty}^{\infty} e^{im\phi_p}\Big\{H_m^{(1)}(k\rho_p)a_m^p + K_m(k\rho_p)b_m^p + \sum_{\substack{k=1\\k\neq p}}^{H}\left[\sum_{n=-\infty}^{\infty} A_{mn}^k(k\rho_p)a_n^k + \sum_{n=-\infty}^{\infty} B_{mn}^k(k\rho_p)b_n^k\right] - J_m(k\rho_p)c_m^p - I_m(k\rho_p)d_m^p + a_m^{(i)}(k\rho_p)\Big\}\Big|_{\rho_p=R_p} = 0, \quad (24)$$

where

$$A_{mn}^k(k\rho_p) = H_{n-m}^{(1)}(kr_{kp})e^{i(n-m)\theta_{kp}}J_m(k\rho_p), \quad (25)$$

$$B_{mn}^k(k\rho_p) = (-1)^m e^{i(n-m)\theta_{kp}}I_m(k\rho_p)K_{n-m}(kr_{kp}). \quad (26)$$

By applying Eq. (7) into Eq. (24), the normal slope continuity condition in the circular boundary B_p $(p=1,\ldots,H)$ is given by

$$\sum_{m=-\infty}^{\infty} e^{im\phi_p}k\Big\{H_m^{(1)\prime}(k\rho_p)a_m^p + K_m'(k\rho_p)b_m^p + \sum_{\substack{k=1\\k\neq p}}^{H}\left[\sum_{n=-\infty}^{\infty} C_{mn}^k(k\rho_p)a_n^k + \sum_{n=-\infty}^{\infty} D_{mn}^k(k\rho_p)b_n^k\right] - J_m'(k\rho_p)c_m^p - I_m'(k\rho_p)d_m^p + b_m^{(i)}(k\rho_p)\Big\}\Big|_{\rho_p=R_p} = 0, \quad (27)$$

where

$$C_{mn}^k(k\rho_p) = H_{n-m}^{(1)}(kr_{kp})e^{i(n-m)\theta_{kp}}J_m'(k\rho_p), \quad (28)$$

$$D_{mn}^k(k\rho_p) = (-1)^m e^{i(n-m)\theta_{kp}}I_m'(k\rho_p)K_{n-m}(kr_{kp}), \quad (29)$$

$$b_m^{(i)}(k\rho_p) = c_p i^m J_m'(k\rho_p)e^{-im\alpha}. \quad (30)$$

Please cite this article as: Lee WM, Chen JT. Scattering of flexural wave in a thin plate with multiple circular inclusions by using the multipole method. International Journal of Mechanical Sciences (2011), doi:10.1016/j.ijmecsci.2011.05.008

Using Eq. (8), the normal bending moment continuity condition in the circular boundary B_p ($p=1, \ldots, H$) yields

$$\sum_{m=-\infty}^{\infty} e^{im\phi_p}\Big\{\alpha_m^H(k\rho_p)a_m^p+\alpha_m^K(k\rho_p)b_m^p + \sum_{\substack{k=1\\k\neq p}}^{H}\Big[\sum_{n=-\infty}^{\infty}E_{mn}^k(k\rho_p)a_n^k+\sum_{n=-\infty}^{\infty}F_{mn}^k(k\rho_p)b_n^k\Big] - \alpha_m^J(k\rho_p)c_m^p-\alpha_m^I(k\rho_p)d_m^p+c_m^{(i)}(k\rho_p)\Big\}\Big|_{\rho_p=R_p}=0, \tag{31}$$

where

$$E_{mn}^k(k\rho_p)=H_{n-m}^{(1)}(kr_{kp})e^{i(n-m)\theta_{kp}}\alpha_m^J(k\rho_p), \tag{32}$$

$$F_{mn}^k(k\rho_p)=(-1)^m e^{i(n-m)\theta_{kp}}\alpha_m^I(k\rho_p)K_{n-m}(kr_{kp}), \tag{33}$$

$$c_m^{(i)}(k\rho_p)=c_p i^m \alpha_m^J(k\rho_p)e^{-im\alpha}, \tag{34}$$

in which the moment operator $\alpha_m^X(k\rho)$ from Eq. (8) is defined as

$$\alpha_m^X(k\rho)=D\Big\{(1-\mu)\frac{X_m'(k\rho)}{\rho}-\Big[(1-\mu)\frac{m^2}{\rho^2}\mp k^2\Big]X_m(k\rho)\Big\}, \tag{35}$$

where the upper (lower) signs refer to $X=J, Y, H, (I, K)$, respectively. The differential equations for the Bessel functions have been used to simplify $\alpha_m^X(k\rho)$.

Similarly, the effective shear operator $\beta_m^X(k\rho)$ derived from Eq. (10) can be expressed as

$$\beta_m^X(k\rho)=D\Big\{\Big[m^2(1-\mu)\pm(k\rho)^2\Big]\frac{X_m'(k\rho)}{\rho^2}-m^2(1-\mu)\frac{X_m(k\rho)}{\rho^3}\Big\}, \tag{36}$$

and the effective shear force continuity condition in the circular boundary B_p ($p=1, \ldots, H$) is given by

$$\sum_{m=-\infty}^{\infty} e^{im\phi_p}\Big\{\beta_m^H(k\rho_p)a_m^p+\beta_m^K(k\rho_p)b_m^p + \sum_{\substack{k=1\\k\neq p}}^{H}\Big[\sum_{n=-\infty}^{\infty}G_{mn}^k(k\rho_p)a_n^k+\sum_{n=-\infty}^{\infty}H_{mn}^k(k\rho_p)b_n^k\Big] - \beta_m^J(k\rho_p)c_m^p-\beta_m^I(k\rho_p)d_m^p+d_m^{(i)}(k\rho_p)\Big\}\Big|\rho_p=R_p=0, \tag{37}$$

where $G_{mn}^k(k\rho_p)$, $H_{mn}^k(k\rho_p)$ and $d_m^{(i)}(k\rho_p)$ are determined by replacing $\alpha_m^X(k\rho_p)$ in Eqs. (35)–(37) with $\beta_m^X(k\rho_p)$, respectively.

Applying the orthogonal property of $\{e^{im\phi_p}\}$ to Eqs. (24), (27), (31) and (37), respectively, gives

$$\begin{cases} H_m^{(1)}(kR_p)a_m^p+K_m(kR_p)b_m^p+\sum\limits_{\substack{k=1\\k\neq p}}^{H}\Big[\sum\limits_{n=-\infty}^{\infty}A_{mn}^k(kR_p)a_n^k+\sum\limits_{n=-\infty}^{\infty}B_{mn}^k(kR_p)b_n^k\Big] \\ \quad -J_m(kR_p)c_m^p-I_m(kR_p)d_m^p=-a_m^{(i)}(kR_p), \\ H_m^{(1)\prime}(kR_p)a_m^p+K_m'(kR_p)b_m^p+\sum\limits_{\substack{k=1\\k\neq p}}^{H}\Big[\sum\limits_{n=-\infty}^{\infty}C_{mn}^k(kR_p)a_n^k+\sum\limits_{n=-\infty}^{\infty}D_{mn}^k(kR_p)b_n^k\Big] \\ \quad -J_m'(kR_p)c_m^p-I_m'(kR_p)d_m^p=-b_m^{(i)}(kR_p), \\ \alpha_m^H(kR_p)a_m^p+\alpha_m^K(kR_p)b_m^p+\sum\limits_{\substack{k=1\\k\neq p}}^{H}\Big[\sum\limits_{n=-\infty}^{\infty}E_{mn}^k(kR_p)a_n^k+\sum\limits_{n=-\infty}^{\infty}F_{mn}^k(kR_p)b_n^k\Big] \\ \quad -\alpha_m^J(kR_p)c_m^p-\alpha_m^I(kR_p)d_m^p=-c_m^{(i)}(kR_p), \\ \beta_m^H(kR_p)a_m^p+\beta_m^K(kR_p)b_m^p+\sum\limits_{\substack{k=1\\k\neq p}}^{H}\Big[\sum\limits_{n=-\infty}^{\infty}G_{mn}^k(kR_p)a_n^k+\sum\limits_{n=-\infty}^{\infty}H_{mn}^k(kR_p)b_n^k\Big] \\ \quad -\beta_m^J(kR_p)c_m^p-\beta_m^I(kR_p)d_m^p=-d_m^{(i)}(kR_p). \end{cases} \tag{38}$$

for $m=0, \pm1, \pm2, \ldots, n=0, \pm1, \pm2, \ldots$, and $p=1, \ldots, H$. Eq. (38) is a coupled infinite system of simultaneous linear algebraic equations which is the analytical model for the flexural scattering of an infinite plate containing multiple circular inclusions. In order to present the numerical results in the following, the infinite system of Eq. (38) is truncated to a $(4H)(2M+1)$ system of equations for $(4H)(2M+1)$ unknown coefficients, i.e. $m=0, \pm1, \pm2, \ldots, \pm M$. Once the coefficients a_m^k, b_m^k, c_m^k and d_m^k($k=1, \ldots, H$; $m=0, \pm1, \pm2, \ldots, \pm M$) are determined, the displacement fields of both an infinite plate and inclusions can be determined by substituting them into Eqs. (12) and (13).

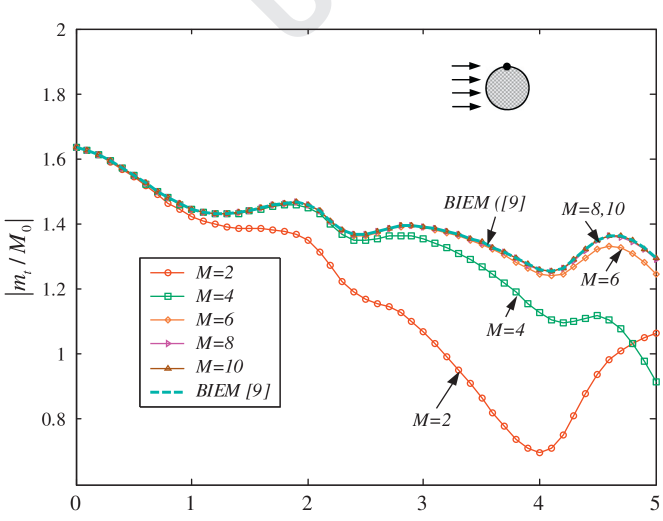

Fig. 2. DMCF on the circular boundary ($\theta=\pi/2$) versus the dimensionless wave number by using different number of coefficients.

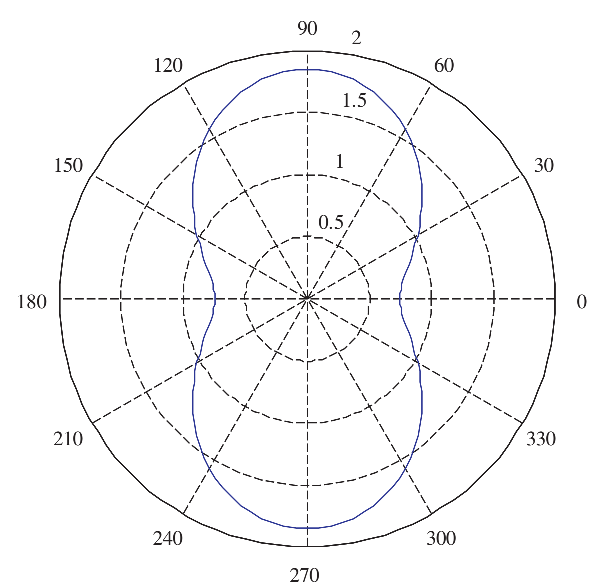

Fig. 3. DMCF along the circular boundary of a flexible inclusion in an infinite plate ($ka=0.005$ and $h/h_0=0.0005$).

3.1. Dynamic moment concentration factors

In the polar coordinates, the bending slope, the normal bending moment, the tangential bending moment and the effective shear force of an infinite plate and each inclusion induced by the incident wave can be determined by substituting Eqs. (12) and (13) into Eqs. (7)–(10), respectively. By setting the amplitude of incident wave to be one ($w_0=1$), the amplitude of normal bending moment produced by the incident wave is

$$M_0 = Dk^2 \tag{39}$$

The dynamic moment concentration factor (DMCF) at any field point $\boldsymbol{x}$ is defined as

$$DMCF(\boldsymbol{x}) = m_t(\boldsymbol{x})/M_0, \tag{40}$$

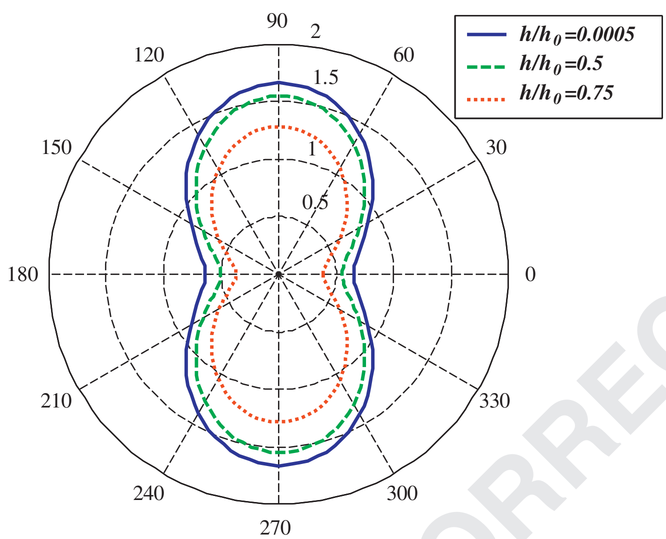

Fig. 4. DMCF along the circular boundary of a flexible inclusion at different thicknesses, solid line for $h/h_0=0.0005$, dashed line for $h/h_0=0.5$ and dotted line for $h/h_0=0.75$ ($ka=0.5$).

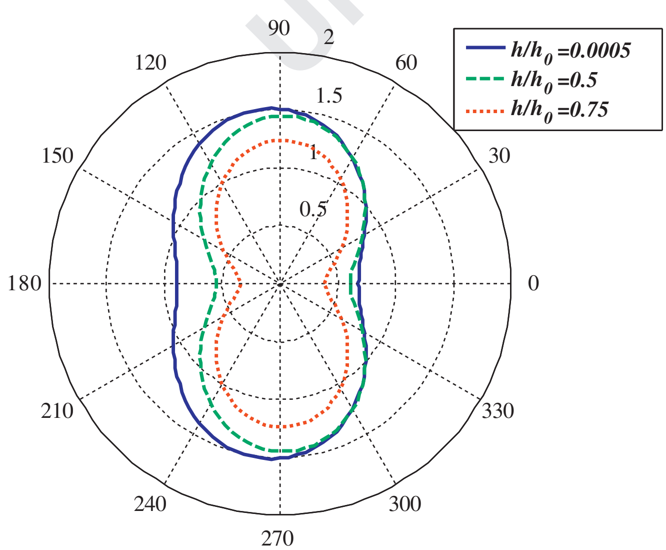

Fig. 5. DMCF along the circular boundary of a flexible inclusion at different thicknesses, solid line for $h/h_0=0.0005$, dashed line for $h/h_0=0.5$ and dotted line for $h/h_0=0.75$ ($ka=1.0$).

where the tangential bending moment $m_t(\boldsymbol{x})$ is determined by the following equations:

$$m_t(\boldsymbol{x};\rho_p,\phi_p) = \begin{cases} \displaystyle\sum_{m=-\infty}^{\infty} e^{im\phi_p}\left\{ f_m^{(i)}(k\rho_p) + \gamma_m^H(k\rho_p)a_m^p + \gamma_m^K(k\rho_p)b_m^p \right. \\ \left. \displaystyle + \sum_{\substack{k=1\\k\neq p}}^{H}\left[\sum_{n=-\infty}^{\infty} \overline{E}_{mn}^k(k\rho_p)a_n^k + \overline{F}_{mn}^k(k\rho_p)b_n^k\right]\right\} & \text{for the plate,} \\ \displaystyle\sum_{m=-\infty}^{\infty} e^{im\phi_p}\{\gamma_m^J(k\rho_p)c_m^p + \gamma_m^I(k\rho_p)d_m^p\}, & \text{for the inclusion,} \end{cases} \tag{41}$$

where $\overline{E}_{mn}^k(k\rho_p)$, $\overline{F}_{mn}^k(k\rho_p)$ and $f_m^{(i)}(k\rho_p)$ are obtained by replacing $\alpha_m^X(k\rho_p)$ in Eqs. (32)–(34) with $\gamma_m^X(k\rho_p)$, respectively, and the tangential bending moment operator $\gamma_m^X(k\rho)$ derived from Eq. (9)

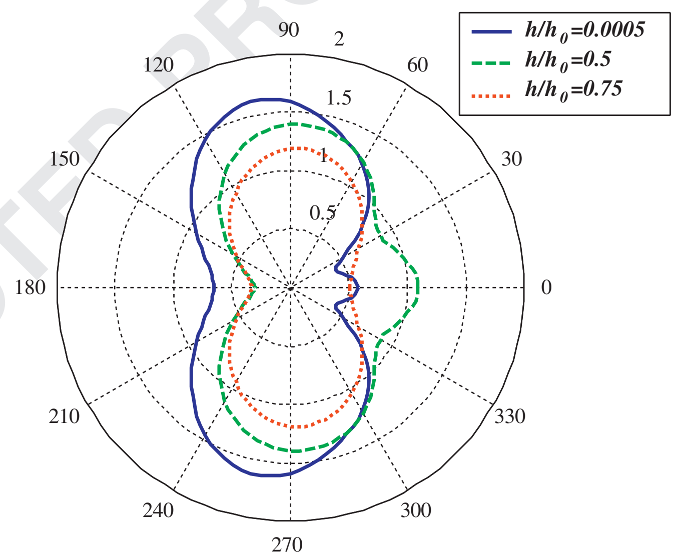

Fig. 6. DMCF along the circular boundary of a flexible inclusion at different thicknesses, solid line for $h/h_0=0.0005$, dashed line for $h/h_0=0.5$ and dotted line for $h/h_0=0.75$ ($ka=3.0$).

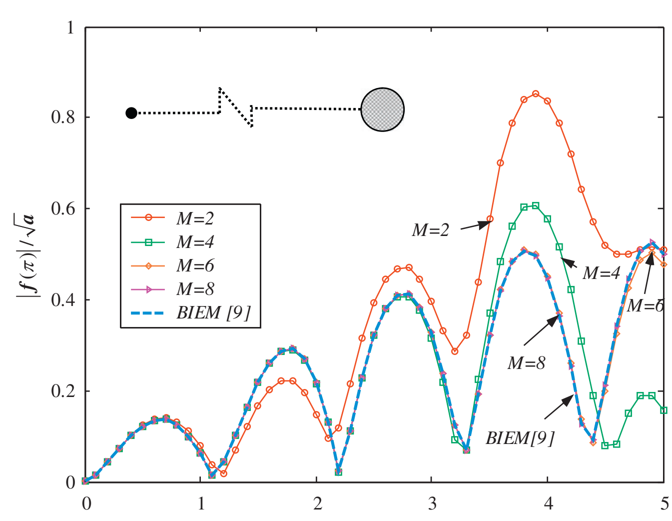

Fig. 7. Far-field backscattering amplitude versus the dimensionless wave number by using different number of coefficients.

Please cite this article as: Lee WM, Chen JT. Scattering of flexural wave in a thin plate with multiple circular inclusions by using the multipole method. International Journal of Mechanical Sciences (2011), doi:10.1016/j.ijmecsci.2011.05.008

is given by

$$\gamma_m^X(k\rho) = D\left\{(\mu-1)\frac{X_m'(k\rho)}{\rho} - \left[(\mu-1)\frac{m^2}{\rho^2} \mp \mu k^2\right] X_m(k\rho)\right\}. \quad (42)$$

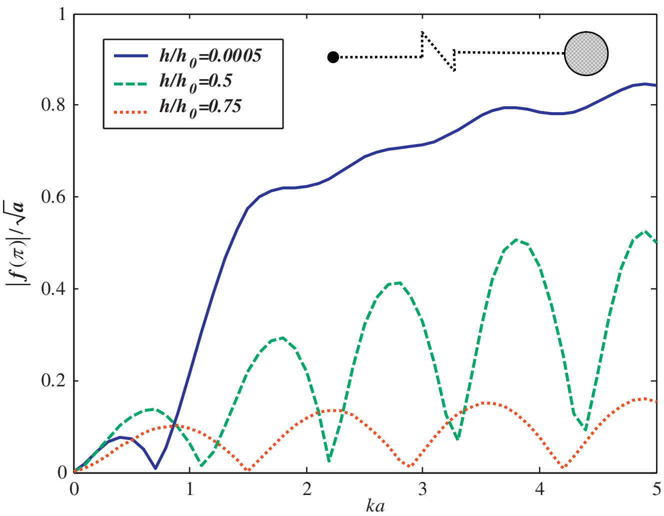

Fig. 8. Far-field backscattering amplitude versus the dimensionless wave number at different thicknesses of a flexible inclusion, solid line for $h/h_0 = 0.0005$, dashed line for $h/h_0 = 0.5$ and dotted line for $h/h_0 = 0.75$.

3.2. Scattered far-field amplitude

For the most part of scattering applications, it is interesting to measure the scattered field far away from the scatterer. On the other hand, the asymptotic behavior or uniqueness of fundamental solutions is an important issue for the numerical computation. Therefore, we examine the behavior of the scattered response in the far field. The scattered far-field amplitude $f(\phi)$ [5] is defined as

$$f(\phi) = \lim_{\rho\to\infty} \sqrt{2\rho} \cdot |w^{(sc)}(\boldsymbol{x})|. \quad (43)$$

In this paper, the radius of the field point is taken as 90 m because $f(\phi)$ converges a steady value when this radius is more than about 90 m.

4. Numerical results and discussions

To demonstrate the theoretical formulation in the previous section, the FORTRAN code was implemented to solve the flexural wave scattered by multiple circular inclusions in an infinite thin plate. The near-field DMCF as well as the far-field scattering amplitude is numerically determined in the truncated finite system from Eq. (38). In all cases, the thickness of plate h_0 is 0.002 m unless otherwise specified. The following dimensionless variables are utilized in the next computation: the incident wave number is ka, the space between inclusions is L/a and the

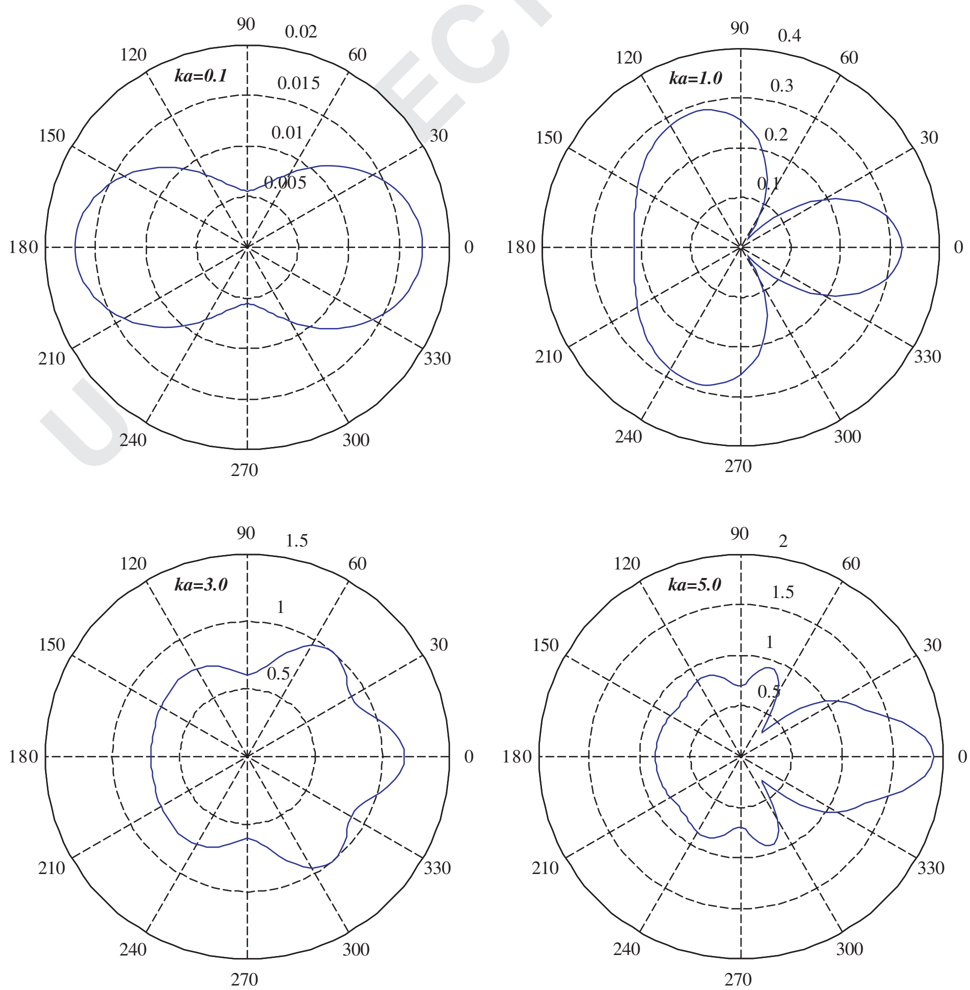

Fig. 9. Far-field scattering pattern for a flexible inclusion with $h/h_0 = 0.0005$ at various dimensionless wave numbers $ka = 0.1$, 1.0, 3.0 and 5.0.

thickness of flexible inclusion is h/h_0, where a is the radius of a circular inclusion and L is the central distance between inclusions. For the special case of a hole, it can be modeled by reducing the value of h/h_0 to be 0.0005 in the numerical simulation.

Case 1: An infinite plate with one circular inclusion:

An infinite plate with one circular flexible inclusion of radius a subject to the incident flexural wave with $\alpha=0$ was firstly considered. Considering a flexible inclusion with $h/h_0=0.5$, Fig. 2 shows the DMCF on the circular boundary, at $\pi/2$, versus the dimensionless wave number by using different number of coefficients. The convergence analysis for one inclusion indicates that the rate of convergence is fast and it essentially depends on the incident flexural wave number for this case. For the case of $ka=0.005$ and $h/h_0=0.0005$, Fig. 3 shows the proposed quasi-static DMCF along the circular boundary of a flexible inclusion. The maximum of DMCF occurs at $\phi=\pi/2, -\pi/2$ and its value is 1.8514, which agrees with the analytical solution of an infinite plate with one hole [1].

Figs. 4–6 show the distribution of DMCF along the circular boundary of a flexible inclusion when the different size of a circular damage ($ka=0.5$, 1.0 and 3.0) and the different corrosion-induced thinning ($h/h_0=0.0005$, 0.5 and 0.75) were considered. When ka or the size of a circular damage is small, the distribution of DMCF has the symmetry of the y-axis. This symmetry gradually becomes broken as ka increases, viz., the size of a circular damage or incident wave number increases. In addition, the distribution of DMCF become skewed toward backward scattering ($h/h_0=0.0005$) from forward scattering ($h/h_0=0.5$) as h/h_0 becomes small and $ka=3.0$. In general, the magnitude of DMCF increases as h/h_0 decreases. However, it is not the case for some azimuthal coordinates like $\phi=0$ when ka is as large as 3.0, indicating that region of the fatigue failure will vary as the size of a circular damage or incident wave number increases.

For the case of one flexible inclusion with $h/h_0=0.5$, Fig. 7 shows the far-field backscattering amplitude versus the dimensionless wave number by using different number of coefficients. The convergence analysis for the far-field backscattering amplitude also shows a fast rate of convergence, where twenty terms of Fourier series in the BIEM are used for comparison. Fig. 8 indicates the far-field backscattering amplitude versus the dimensionless wave number when three different dimensionless thicknesses of inclusion ($h/h_0=0.0005$, 0.5 and 0.75) were considered. As h/h_0 increases, the ka occurring at first trough increases, the far-field

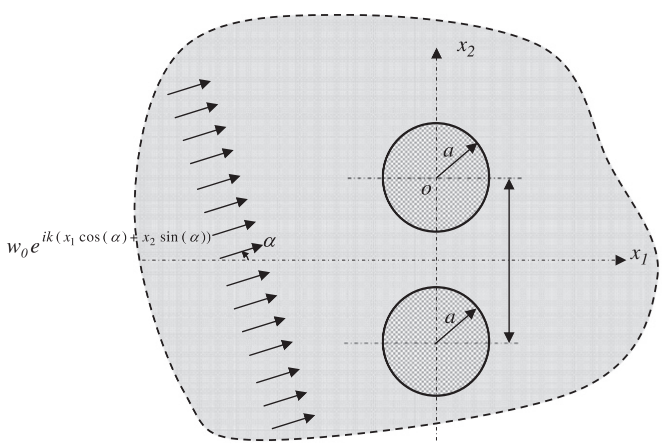

Fig. 10. An infinite thin plate with two circular inclusions subject to an incident flexural wave with an incident angle α

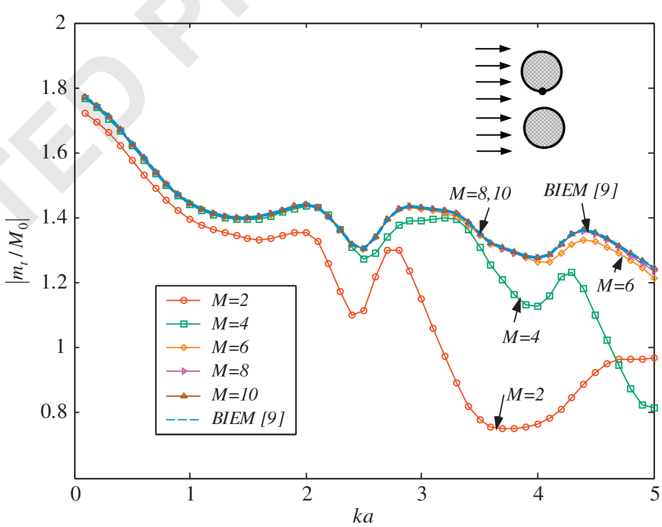

Fig. 12. DMCF on the upper circular boundary ($\theta=-\pi/2$) versus the dimensionless wave number by using different number of coefficients ($L/a=4.0$).

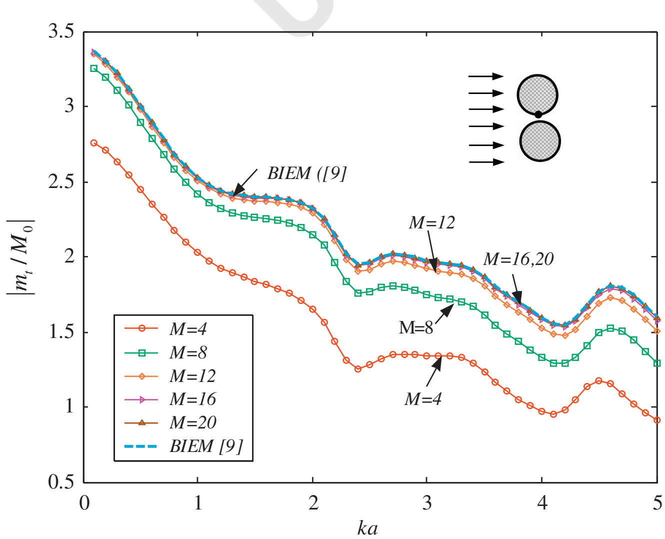

Fig. 11. DMCF on the upper circular boundary ($\theta=-\pi/2$) versus the dimensionless wave number by using different number of coefficients ($L/a=2.1$).

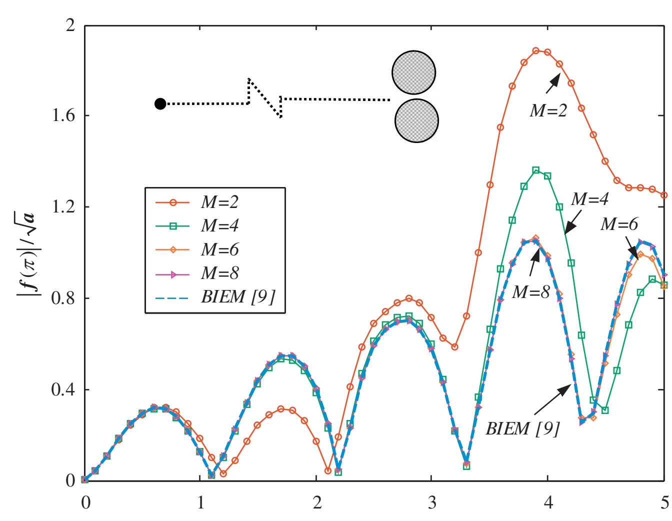

Fig. 13. Far-field backscattering amplitude versus the dimensionless wave number by using different number of coefficients ($L/a=2.1$).

Please cite this article as: Lee WM, Chen JT. Scattering of flexural wave in a thin plate with multiple circular inclusions by using the multipole method. International Journal of Mechanical Sciences (2011), doi:10.1016/j.ijmecsci.2011.05.008

amplitude decreases and oscillates with ka. The proposed results match well with those of Norris and Vemula [5]. It can be found that the scattering amplitude in the far field is O $(\rho^{-1/2})$ to satisfy the radiation condition. Fig. 9 shows the far-field scattering pattern for a flexible inclusion with $h/h_0=0.0005$ at various dimensionless wave numbers $ka=0.1$, 1.0, 3.0 and 5.0. Some results ($ka=1.0$ and 5.0) match well with those of Norris and Vemula [5]. It indicates that the scattering patterns vary appreciably as the size of a circular damage or incident wave number increases.

Case 2: *An infinite plate with two circular inclusions*:

A case of an infinite thin plate with two identical flexible circular inclusions subject to the incident flexural wave with an incident angle α was considered in Fig. 10. Taking $\alpha=0$ was investigated in the following computation. Figs. 11–14 show the convergence analysis for the near-field DMCF and the far-field scattering amplitude, respectively, when the different dimensionless central distance ($L/a=2.1$ and 4.0) were considered. Fig. 11 shows DMCF on the upper circular boundary ($\theta=-\pi/2$) versus the dimensionless wave number by using different number of coefficients when $L/a=2.1$. It indicates that the convergence is fast achieved as the value of M increases. The proposed results with $M=20$ match well with those provided by the BIEM [9] in which thirty terms of Fourier series are used. Compared with the convergence analysis in [9], the fictitious frequency appearing in the BIEM [9] does not appear in the present formulation. During the convergence analysis, the maximum of the allowable truncated number M is limited by the minimum value of ka concerned, for instance here $ka=0.1$. The reason for this is that the Bessel functions of $Y_m(kR_p)$ and $I_m(kR_p)$ of Eq. (38) become large when k is small. Actually, the truncated number M can be increased while the concerned minimum value of ka increases. When the value of L/a increases to 4.0 as shown in Fig. 12, the rate of convergence becomes faster and the required truncated number M can be reduced, where twenty terms of Fourier series in the BIEM are used for comparison.

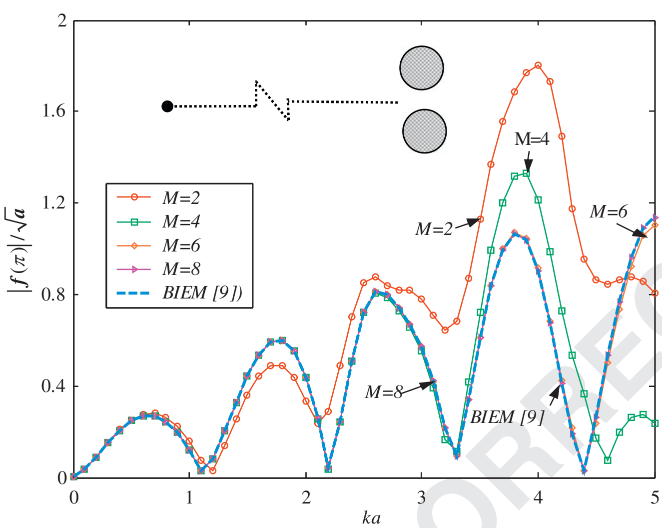

Fig. 14. Far-field backscattering amplitude versus the dimensionless wave number by using different number of coefficients ($L/a=4.0$).

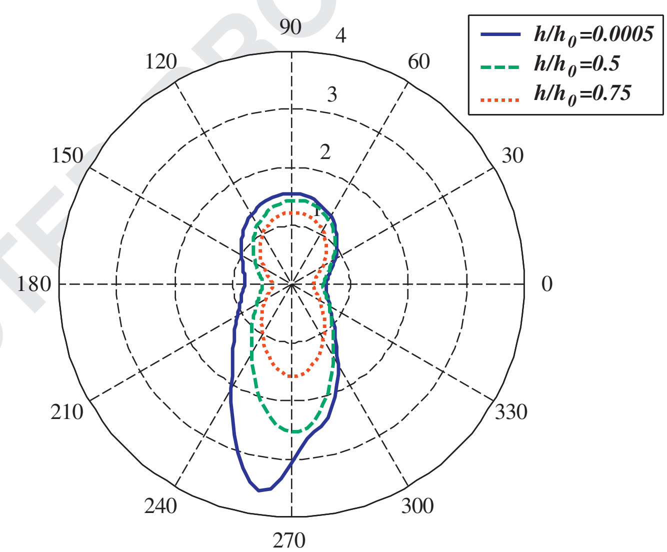

Fig. 16. DMCF along the circular boundary of the upper flexible inclusion at different thicknesses, solid line for $h/h_0=0.0005$, solid line for $h/h_0=0.0005$, dashed line for $h/h_0=0.5$ and dotted line for $h/h_0=0.75$ ($ka=1.0$ and $L/a=2.1$).

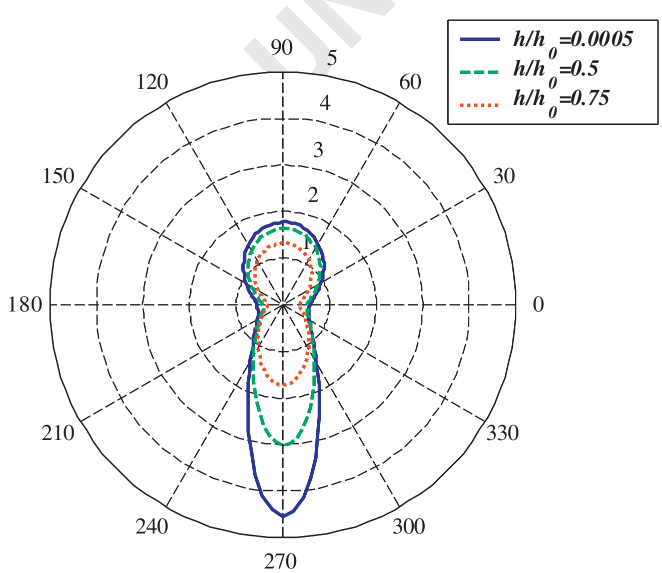

Fig. 15. DMCF along the circular boundary of the upper flexible inclusion at different thicknesses, solid line for $h/h_0=0.0005$, solid line for $h/h_0=0.0005$, dashed line for $h/h_0=0.5$ and dotted line for $h/h_0=0.75$ ($ka=0.5$ and $L/a=2.1$).

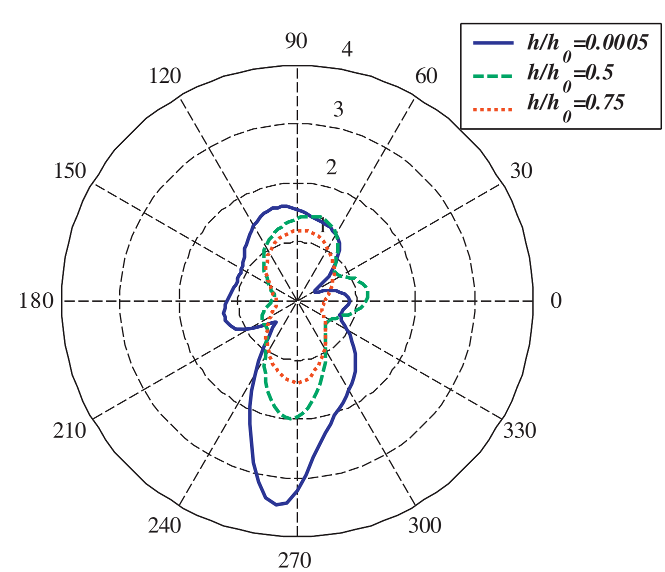

Fig. 17. DMCF along the circular boundary of the upper flexible inclusion at different thicknesses, solid line for $h/h_0=0.0005$, dashed line for $h/h_0=0.5$ and dotted line for $h/h_0=0.75$ ($ka=3.0$ and $L/a=2.1$).

Please cite this article as: Lee WM, Chen JT. Scattering of flexural wave in a thin plate with multiple circular inclusions by using the multipole method. International Journal of Mechanical Sciences (2011), doi:10.1016/j.ijmecsci.2011.05.008

The corresponding convergence analysis for the far-field scattering amplitude is shown in Figs. 13 and 14, where twenty terms of Fourier series in the BIEM are used for comparison. It indicates that the required number of M is unrelated to the value of L/a. In addition, it can be seen that the convergence rate of the far-field is faster than that of the near field. The complicated calculation for the near-field DMCF can account for this fact. In summary, for the near-field DMCF, when the value of L/a is small, the required number of M mainly depends on the considered minimum dimensionless central distance L/a. When the value of L/a is large (such as 4.0 or 10.0) or one inclusion is considered, the value of M can be reduced and depends on the value of ka of the incident wave. Through the numerical experiments, it is found that the required number of M can be taken from 20 to 8 for the minimum separation distance L/a ranged from 2.1 to 10.0. As regards the far field, taking $M=8$ or 10 can make results accurate enough.

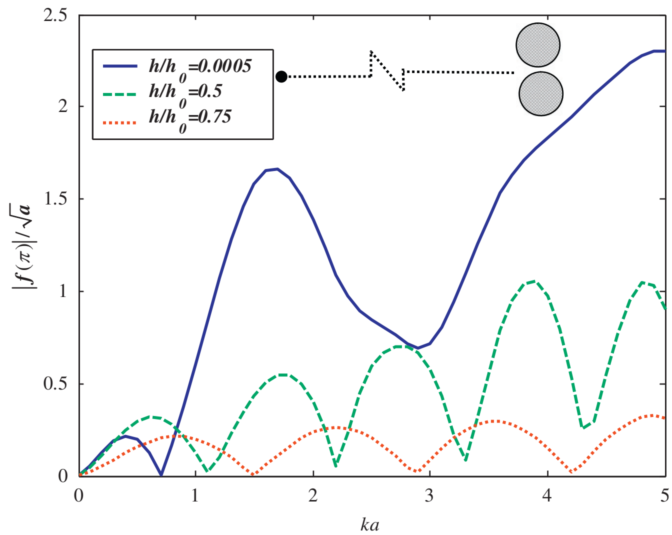

Fig. 18. Far-field backscattering amplitude versus the dimensionless wave number at different thicknesses of a flexible inclusion, solid line for $h/h_0=0.0005$, dashed line for $h/h_0=0.5$ and dotted line for $h/h_0=0.75$ ($L/a=2.1$).

For the case of $L/a=2.1$, Figs. 15–17 show the distribution of DMCF along the circular boundary of the upper flexible inclusion when the different size of a circular damage ($ka=0.5$, 1.0 and 3.0) and the different corrosion-induced thinning ($h/h_0=0.0005$, 0.5 and 0.75) were considered. It is observed that the distribution of DMCF of two circular inclusions is different from that of one, where the maximum of DMCF increases nearly three times since the two inclusions are close to each other. This high dynamic stress concentration inevitably results in the fatigue failure of engineering structures and this region should be taken care in the design phase. The variation of DMCF along the azimuthal coordinate is significant when ka or the size of a circular damage increases. Comparing with the result of one inclusion shown in Fig. 8, the more intensity of the far-field backscattering is observed in Fig. 18 and in general the tendency is comparable but the case of the hole. For the case of $L/a=2.1$, Fig. 19 shows the variation of far-field scattering patterns of two flexible inclusions

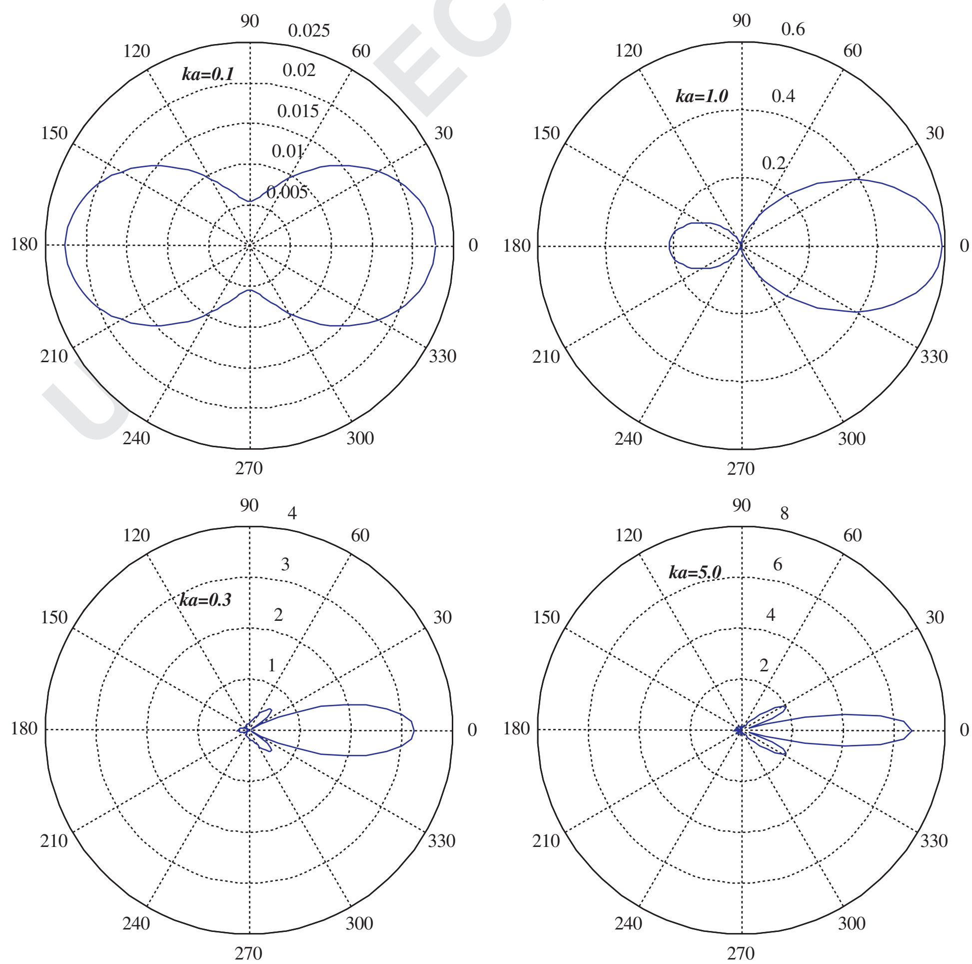

Fig. 19. Far-field scattering pattern for two flexible inclusions with $h/h_0=0.7$ and $L/a=2.1$ at various dimensionless wave numbers $ka=0.1$, 1.0, 3.0 and 5.0.

Please cite this article as: Lee WM, Chen JT. Scattering of flexural wave in a thin plate with multiple circular inclusions by using the multipole method. International Journal of Mechanical Sciences (2011), doi:10.1016/j.ijmecsci.2011.05.008

with a corrosion-induced 30% reduction in thickness, as the size of a circular damage or incident wave number increases ($ka=0.1$, 1.0, 3.0 and 5.0). Comparing with the results of one inclusion shown in Fig. 9, the larger intensity of the far-field scattering is observed. The scattering patterns vary considerably and become more skewed towards forward scattering as ka increases.

In the case of $L/a=4.0$, Figs. 20–22 show the distribution of DMCF along the circular boundary of the upper flexible inclusion when the different size of a circular damage ($ka=0.5$, 1.0 and 3.0) and the different corrosion-induced thinning ($h/h_0=0.0005$, 0.5 and 0.75) were considered. Comparing Fig. 4 with 20, the central distance is large enough so that the DMCF distribution of two inclusions is similar to that of one. But the characteristics of far-field are not the case. From viewing Figs. 8, 18 and 23, the far-field backscattering amplitude of $L/a=4.0$ is similar to that of $L/a=2.1$ rather than that of one inclusion. Similar results for the

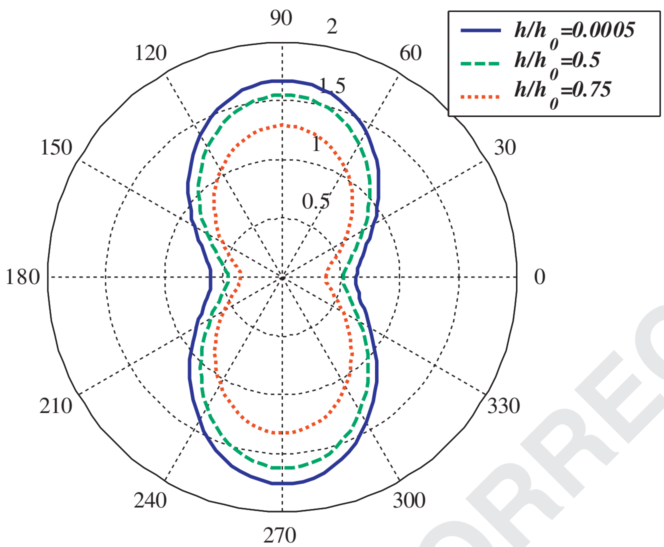

Fig. 20. DMCF along the circular boundary of the upper flexible inclusion at different thicknesses, solid line for $h/h_0=0.0005$, dashed line for $h/h_0=0.5$ and dotted line for $h/h_0=0.75$ ($ka=0.5$ and $L/a=4.0$).

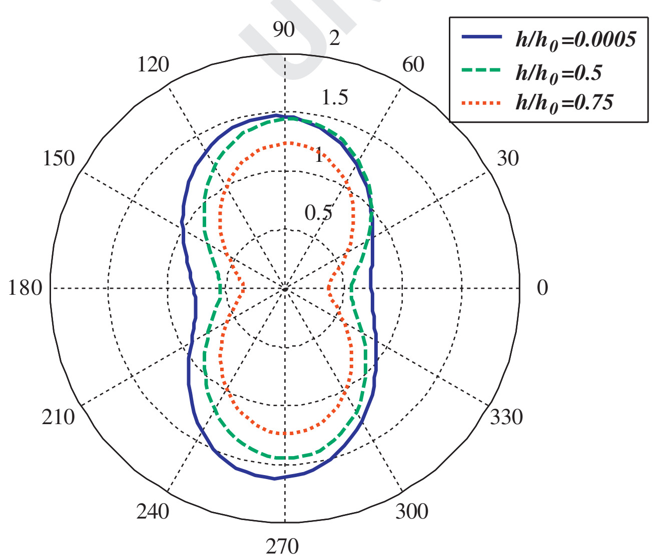

Fig. 21. DMCF along the circular boundary of the upper flexible inclusion at different thicknesses, solid line for $h/h_0=0.0005$, dashed line for $h/h_0=0.5$ and dotted line for $h/h_0=0.75$ ($ka=1.0$ and $L/a=4.0$).

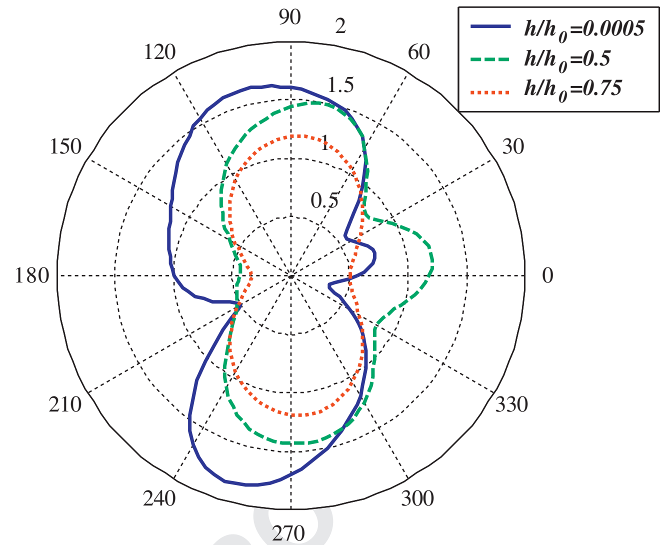

Fig. 22. DMCF along the circular boundary of the upper flexible inclusion at different thicknesses, solid line for $h/h_0=0.0005$, dashed line for $h/h_0=0.5$ and dotted line for $h/h_0=0.75$ ($ka=3.0$ and $L/a=4.0$).

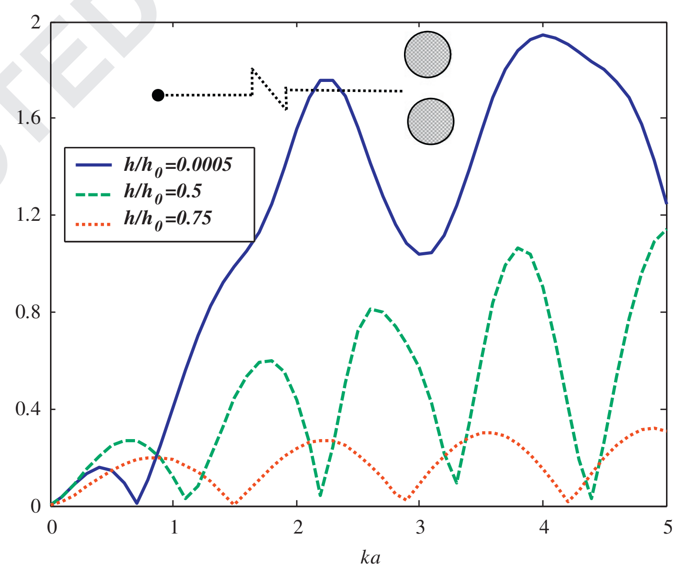

Fig. 23. Far-field backscattering amplitude versus the dimensionless wave number at different thicknesses of a flexible inclusion, solid line for $h/h_0=0.0005$, dashed line for $h/h_0=0.5$ and dotted line for $h/h_0=0.75$ ($L/a=4.0$).

variation of the far-field scattering pattern as ka increases can be seen from Figs. 9, 19 and 24.

As seen from the numerical results shown above, it indicates that the effect of the space between inclusions on the near-field DMCF is different from that on the far-field scattering pattern. Only when concerning the DMCF, the multiple scattering can be simplified by the simple scattering while the space between inclusions is large enough. But the prediction of the far-field multiple scattering cannot do such simplification.

5. Concluding remarks

The flexural wave scattered by multiple circular inclusions or structural anomalies in a plate-like structure has been

Please cite this article as: Lee WM, Chen JT. Scattering of flexural wave in a thin plate with multiple circular inclusions by using the multipole method. International Journal of Mechanical Sciences (2011), doi:10.1016/j.ijmecsci.2011.05.008

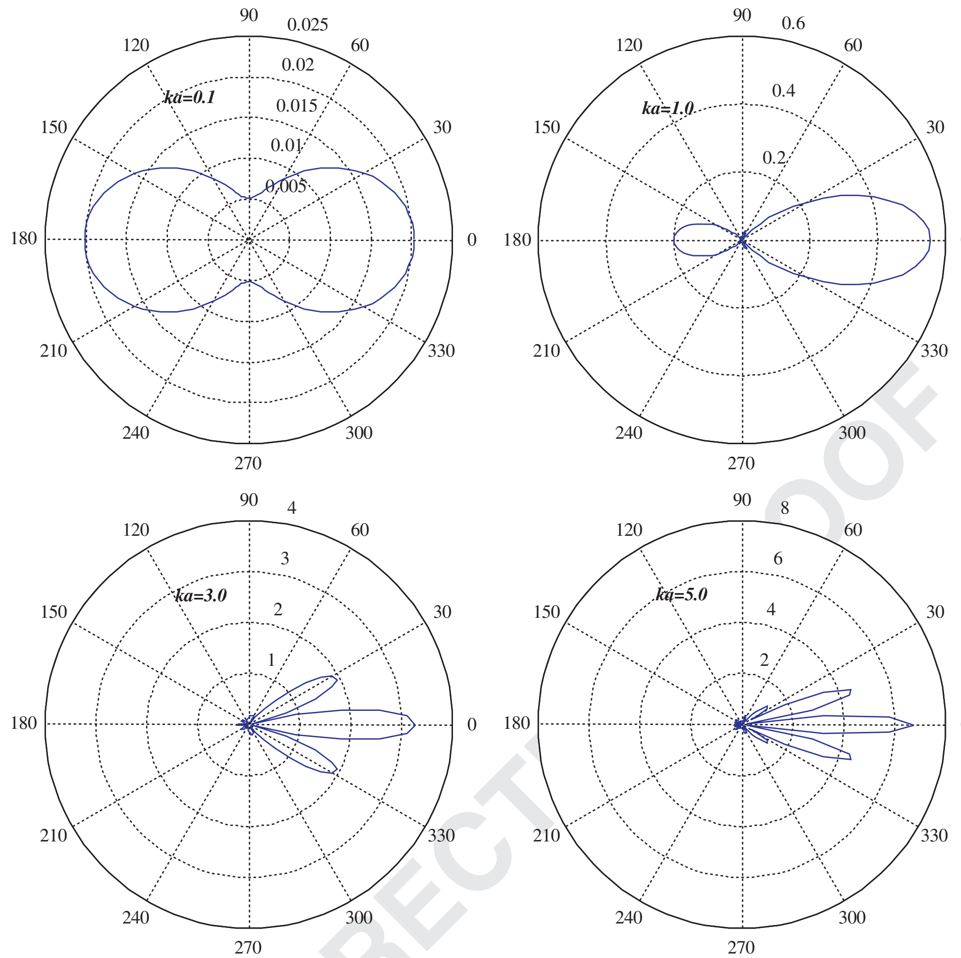

Fig. 24. Far-field scattering pattern for two flexible inclusions with $h/h_0=0.7$ and $L/a=4.0$ at various dimensionless wave numbers $ka=0.1$, 1.0, 3.0 and 5.0.

successively solved by using the multipole method with the aid of the addition theorem. The near-field DMCF and the far-field scattering pattern were mainly concerned in this study. The former is important in the mechanical design in particular for the fatigue failures and the latter can be applicable to the structural health-monitoring system to detect the structural damage. The convergence analyses of these two parameters were conducted by using different numbers of coefficient in the multipole expansion. These results can be employed as guide lines for the usage of the proposed method. Numerical results show that the scattering patterns vary significantly as the size and thickness of a circular damage change, indicating the importance of the scattering pattern to detect the size and severity of structural anomaly in plate structures. In addition, the distribution of DMCF of two damages is different from that of one, where the maximum of DMCF increases nearly three times, indicating the importance of the dynamic stress concentration to avoid from fatigue failures. The magnitude of DMCF is mainly depends on the separating space of damage and next on the incident wave number and its incident angle. The effect of the space between inclusions on the near-field DMCF is different from that on the far-field scattering. This finding is helpful to further study the multiple scattering of flexural wave.

References

[1] Pao YH, Mow CC. Diffraction of elastic waves and dynamics stress concentration. New York: Crane-Russak; 1972.
[2] Nishimura G, Jimbo Y. A dynamical problem of stress concentration. Journal of the Faculty of Engineering, University of Tokyo, Japan 1955;24:101.
[3] Pao YH. Dynamical stress concentration in an elastic plate. Transactions of the ASME Journal of Applied Mechanics 1962;29:299–305.
[4] Thau SA, Lu TH. Dynamic stress concentration at a cylindrical inclusion in an elastic medium with an arbitrarily stiff bond. International Journal of Mechanical Sciences 1969;11(8):677–88.
[5] Norris AN, Vemula C. Scattering of flexural waves on thin plates. Journal of Sound and Vibration 1995;181(1):115–25.
[6] Squire VA, Dixon TW. Scattering of flexural waves from a coated cylindrical anomaly in a thin plate. Journal of Sound and Vibration 2000;236(2):367–73.
[7] Wang CH, Chang FK. Scattering of plate waves by a cylindrical inhomogeneity. Journal of Sound and Vibration 2005;282:429–51.
[8] Peng SZ. Flexural wave scattering and dynamic stress concentration in a heterogeneous plate with multiple cylindrical patches by acoustical wave propagator technique. Journal of Sound and Vibration 2005;286:729–43.
[9] Lee WM, Chen JT. Scattering of flexural wave in a thin plate with multiple circular inclusions by using null-field integral equation approach. Journal of Sound and Vibration 2010;329:1042–61.
[10] Záviška F. Über die Beugung elektromagnetischer Wellen an parallelen, unendlich langen Kreiszylindern. Annalen der Physik, 4 Folge 1913;40:1023–56.
[11] Linton CM, Evans DV. The interaction of waves with arrays of vertical circular cylinders. Journal of Fluid Mechanics 1999;215:549–69.
[12] Watson GN. A treatise on the theory of Bessel functions.2nd ed Cambridge: Cambridge Library Edition; 1995.

Please cite this article as: Lee WM, Chen JT. Scattering of flexural wave in a thin plate with multiple circular inclusions by using the multipole method. International Journal of Mechanical Sciences (2011), doi:10.1016/j.ijmecsci.2011.05.008